LOW FREQUENCY DYNAMICS OF THE BI-STABLE WAKE FOR A THREE-DIMENSIONAL HILL

Daniel MacGregor
Institute for Aerospace Studies
University of Toronto
4925 Dufferin St. ON M3H 5T6 CANADA
daniel.macgregor@mail.utoronto.ca

Philippe Lavoie
Institute for Aerospace Studies
University of Toronto
4925 Dufferin St. ON M3H 5T6 CANADA
phil.lavoie@utoronto.ca

ABSTRACT

The low frequency dynamics of the bi-stable wake for a three-dimensional hill geometry were characterized through experiments at the University of Toronto Institute for Aerospace Studies. Measurements collected in these experiments included long duration unsteady surface-pressure, single-wire hot-wire anemometry (HWA) and stereoscopic particle image velocimetry (PIV). Proper orthogonal decomposition of the unsteady surface-pressure measurements identified the bi-stable component of the wake and a periodic breathing of the recirculation region. The switching between bi-stable states was tracked for a sweep of yaw angles around 0° and found to persist over a 4.5° range. Over this span, the average residence time scale for the bi-stable states ranged from $\mathcal{O}(10^2 - 10^4)$ times the convective time scale, and varied non-monotonically with Reynolds number at a fixed yaw angle. The switching between bi-stable states behaved randomly as a stationary Markov chain. Two low frequency phenomena were identified at $\mathrm{St}_h = 0.065$ and 0.65 through HWA and PIV measurements of separated shear layer on the leeward side of the hill. The lower frequency phenomenon is associated with the breathing of the recirculation region, where the flow field measurements capture the vertical movement of the separated shear layer. The higher frequency feature is linked to the development of an instability within the separated shear layer.

INTRODUCTION

The BeVERLI Hill geometry was developed to further our understanding of three-dimensional (3D) turbulent boundary layers (Gargiulo *et al.*, 2020). Previous experiments at several facilities with the BeVERLI Hill at the orientation of 0° have found that wake to be bi-stable asymmetric under nominally symmetric inflow conditions (Duetsch-Patel *et al.*, 2022; MacGregor *et al.*, 2023; MacGregor & Lavoie, 2024). Furthermore, this bi-stability was found to be aperiodic with a time scale $\mathcal{O}(10^3)$ times the convective time scale.

As highlighted by Williams & Smits (2024) in their review, numerous geometries have been found to develop asymmetries under nominally symmetric flow conditions. Furthermore, the bi-stability seen with the BeVERLI Hill has also been observed with other geometries, most notably with the square backed Ahmed body. Grandemange *et al.* (2013*b*) identified that the bi-stability seen on the Ahmed body will develop once a critical ground clearance is exceeded. After this criterion is reached, whether the bi-stability develops on the lateral or top-bottom edges depends on the model's aspect ratio. They also found at low ground clearances, where the underflow was weak enough for the body to be considered wall mounted, that the lateral bi-stability will develop. This latter set of conditions is similar to those for the BeVERLI Hill.

The low frequency dynamics of the bi-stable wake seen on the Ahmed body have been studied in detail. Grandemange *et al.* (2013*a*) found the lateral and top-bottom pairs of edges each produce shear layer oscillations at about $\mathrm{St}_h \approx 0.17$ (h being the height of the body). Additionally, the switching between bi-stable states was found to be random, behaving as a stationary Markov chain with time scale $\mathcal{O}(10^3)$. Volpe *et al.* (2015) and Haffner *et al.* (2020) found the bi-stability to persist over a 1° range. They also identified a low frequency breathing of the recircualtion region at $\mathrm{St}_w \approx 0.07$ (w is the model width), which matches that first reported by Berger *et al.* (1990) for the flow past circular disks.

The focus of this paper is to characterize experimentally the low frequency dynamics of the bi-stable wake seen on the BeVERLI Hill at 0°. Long duration unsteady surface-pressure, single-wire hot-wire anemometry (HWA) and stereoscopic particle image velocimetry (PIV) are used to identify these features. Coherent features will be compared against those found in the literature for other geometries .

EXPERIMENTAL SETUP

The BeVERLI Hill is defined by a fifth-degree polynomial that is traced around a modified super-elliptical profile. Constraints are applied at the base and peak of the hill, such that the first and second derivatives of the polynomial are equal to zero. All dimensions of the hill are expressed in terms of the hill height, h, allowing for the hill to be scaled to a desired size by assigning a lengthscale to h. A sketch of the BeVERLI Hill

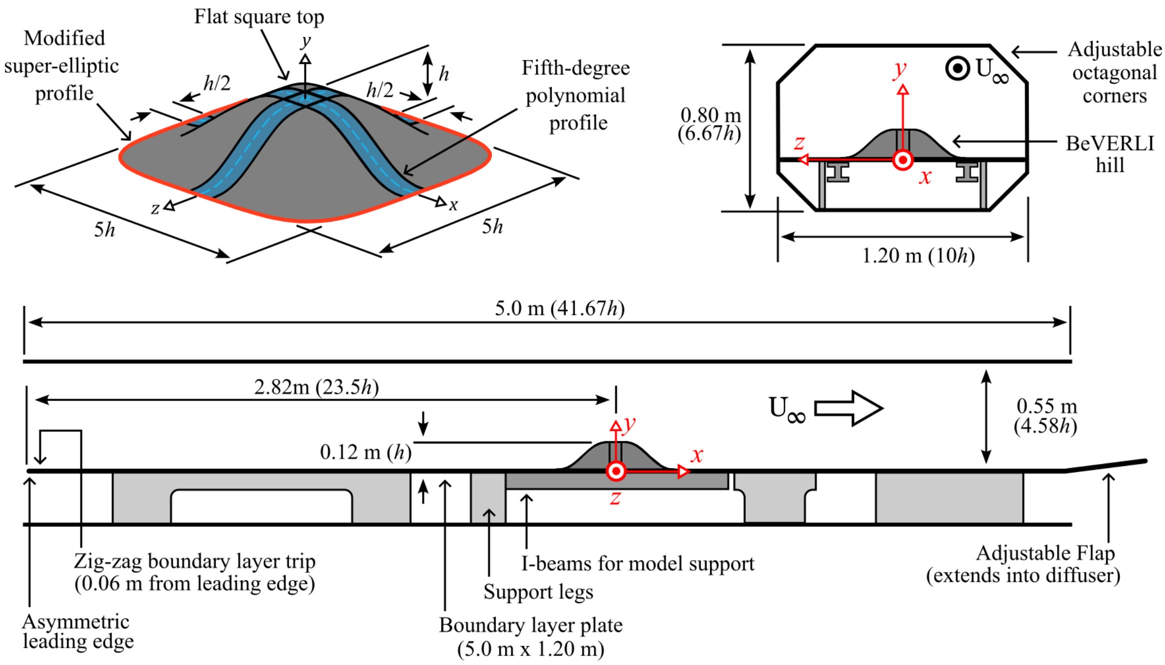

Figure 1. Sketches of the BeVERLI Hill and experimental setup used in the recirculating wind tunnel at UTIAS. Starting from the top left and proceeding in a clockwise order, a sketch of the BeVERLI Hill, a cross-sectional view of the experimental setup and a side view of the experimental setup. Major dimensions and notable features within each sketch are also labelled.

is provided in Figure 1. The hill has four-fold symmetry resulting in it having unique yaw angle orientations relative to the oncoming freestream flow, ψ, over a 90° range that then repeat with every 90° rotation of the hill. A more detailed overview of the BeVERLI Hill design is provided by Gargiulo *et al.* (2020).

The University of Toronto Institute for Aerospace Studies (UTIAS) version of the BeVERLI Hill has a height $h = 0.12$ m and is integrated into a circular base to allow for adjustments in its orientation relative to the incoming flow. A series of 135 pressure taps are arranged in radial lines extending from the model centre such that half the hill was densely tapped with lines at 15° increments while the other half was sparsely tapped at 45° increments. The hill and its base was machined from a single block of 6061 aluminum and anodized in a matte black finish.

Experiments were conducted using the recirculating wind tunnel at UTIAS, which has a test section volume of 5.0 m × 1.2 m × 0.8 m (length × width × height). The test section corners are fitted with fillets that can be adjusted to maintain a nominal zero-pressure gradient flow. The tunnel is capable of producing flow speeds up to 40 m/s with freestream turbulence intensity of 0.08% (Hearst, 2015). The experiments in this study used a boundary layer plate setup that spans the full length and width of the test section and reduce the effective test section height to 0.55 m. The BeVERLI Hill is placed 2.82 m downstream of the leading edge. Flow attachment on the testing side of the plate is maintained through adjustment of a flap at the plate trailing edge. A zig-zag trip is placed 0.06 m downstream of the leading edge to trigger the development of a uniform turbulent boundary layer. The origin of the global coordinate system is positioned at the hill centre in the ground plane. The x-axis is aligned with the freestream velocity vector, and y-axis is oriented upward normal to the ground plane. Changes in ψ are made by rotating the hill about the y-axis following right-hand rotation convention. A sketch of the experimental setup is provided in Figure 1.

The hill height based Reynolds, $\mathrm{Re}_h = U_\infty h/\nu$, tested ranged from 38,000 to 250,000. At 5.5h upstream of the hill centre, the hill height to boundary layer ratio, h/δ varied from 2.84 to 3.86 for $\mathrm{Re}_h = 38,000$ to $208,000$, respectively. Unsteady surface-pressure measurements were collected at a rate of 100 Hz using an in-house 40 sensor 2 kPa array and a MKS120AD Baratron with sensing ranges of 1 Torr and 10 Torr. Similar measurements were also collected at a select number of ports using 1 psi Endevco transducers at a sampling rate of 16,000 Hz. Tubing lengths from the in-house array and Baratron were set to be 0.9 m while it was 0.3 m for the Endevco transducer. Point measurements of the velocity in the wake were conducted using a single hot-wire probe operated by a Dantec Streamware anemometer. Flow field measurements were obtained also using stereoscopic PIV. Images were captured using two LaVision 16-bit 5.5 megapixel sCMOS cameras and processed into vector fields using DaVis 11.0.

RESULTS & DISCUSSION

POD of Unsteady Surface-Pressure

The BeVERLI Hill was oriented at the nominal position of 0° such that the densely tapped half of the hill was located on the leeward face of the hill. Of these taps, 40 were used to collect surface-pressure readings over periods $\mathcal{O}(10^5)$ times the convective time scale of the flow, h/U_∞. Proper orthogonal decomposition (POD) was performed to identify large-scale features of the surface-pressure field. The first four modes, their proportions of the total energy, and the power-spectral-density (PSD) of their time coefficients are presented in Figure 2 for $\mathrm{Re}_h = 165,000$ at $\psi = 1.1°$. The purpose of the small yaw angle was to have the flow be in a 50-50 split between bi-stable states, whereas at 0°, the ratio was uneven. The effect of ψ on the bi-stability is explored in next section.

The first POD mode captures the bi-stability which contains approximately 55% of the total energy. The large scale

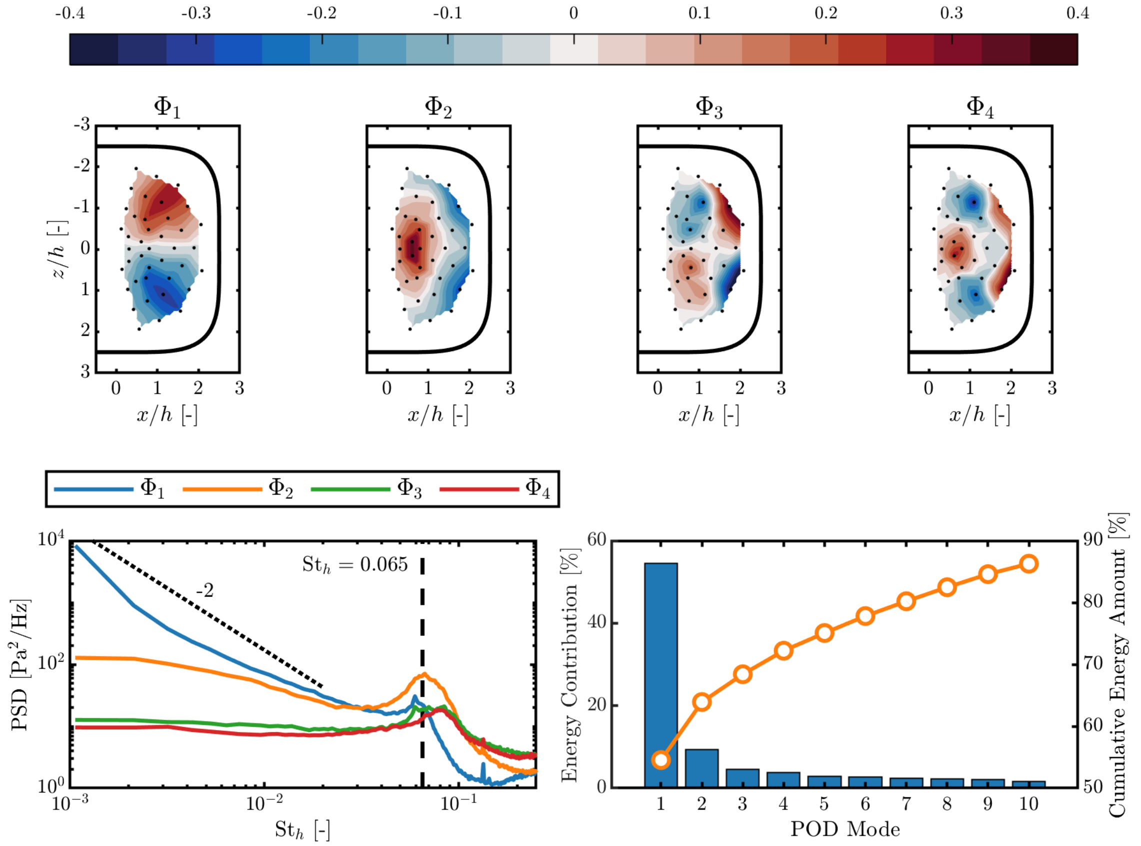

Figure 2. POD of unsteady surface pressure measurements collected on the leeward face of the BeVERLI Hill for $\mathrm{Re}_h = 165,000$ at $\psi = 1.1°$, which gives a 50-50 split between the bi-stable states. The top row of figures shows the first four POD spatial modes (from left to right). The line plot on the bottom left shows the PSD of time coefficients for each POD mode with the -2 frequency relation compared against the first mode, and the peak at $\mathrm{St}_h = 0.065$ for the second mode indicated. The bottom right mode shows the energy distribution for the first ten modes and the cumulative total energy with each mode.

fluctuations of this mode are positioned along the 45° radial lines of taps. This spatial mode matches that seen by MacGregor *et al.* (2023) with the same model tested at Virginia Tech for $\mathrm{Re}_h = 250,000$, where it too was the most energetic mode, but contributed only 33% energy to the total. When examining the time coefficients for this mode, it was found to alternate between two levels, where it would remain at either level for long periods, $\mathcal{O}(10^3)$ times the convective time scale, before switching to the other level. Volpe *et al.* (2015) observed similar behaviour in POD of unsteady surface-pressure measurements with the Ahmed body, where this mode was found to capture the bi-stable component of the wake. The PSD of the time coefficients for this mode shows that a large amount of energy is contained at frequencies below 1 Hz. Within this region, the PSD decreases at a near exponential rate; a characteristic of random processes. This low-frequency behaviour is similar to the behaviour observed with the bi-stability on the Ahmed body as noted by Grandemange *et al.* (2013*a*) and Volpe *et al.* (2015), where they saw this behaviour follow a $1/f^2$ trend (f being frequency in Hz).

The second most energetic mode contains approximately 10% of the total energy and captures a periodic breathing of the recirculation region. The PSD of the time coefficients for this mode reveals a strong peak at a Strouhal number, $\mathrm{St}_h = fh/U_\infty \approx 0.065$. The breathing of the recirculation region matches findings by Berger *et al.* (1990) for flows around circular disks ($\mathrm{St}_d = 0.07$ with d being the disk diameter) and Volpe *et al.* (2015) and Haffner *et al.* (2020) with the Ahmed body ($\mathrm{St}_w \approx 0.07$). After the second mode, the energy contribution drops off significantly with the next mode containing less than 5% of the total energy. The third and fourth mode capture weaker lateral instabilities at $\mathrm{St}_h \approx 0.08$.

Tracking the bi-stability

A simple method to track the bi-stability was developed that uses two ports on the 45° lines of the leeward face that are at mirror symmetric positions relative to the model centerline. The difference in pressure between the ports is calculated as $\Delta p = p_+ - p_-$, where p_+ denotes the pressure measured on the $+z$ side of the hill and vice versa for p_-. Alternatively, this pressure difference can be measured directly by connecting the total and static sides to the $+z$ and $-z$ pressure taps, respectively. For theses experiments, the direct approach was used. The histogram of Δp is bimodal where each peak is associated with a bi-stable state of the flow. The tracking parameter is computed by applying the mid-value and range between these peaks to the original signal to centre the histogram about zero and normalize it, respectively. This results in an adjusted version of Δp where its histogram peaks are now at ± 1.

This new signal can be traced to identify when the flow switches between bi-stable states. A switch is deemed to have occurred if the signal crosses zero and reaches a magnitude of one before its next zero crossing. To differentiate the two bi-stable states, when the signal has a positive sign, it is denoted as the $\mathcal{P}$ state and vice versa for the $\mathcal{N}$ state. This aligns with flowfield results by MacGregor & Lavoie (2024), where the centroid of the recirculation region is on the $+z$ side of the hill

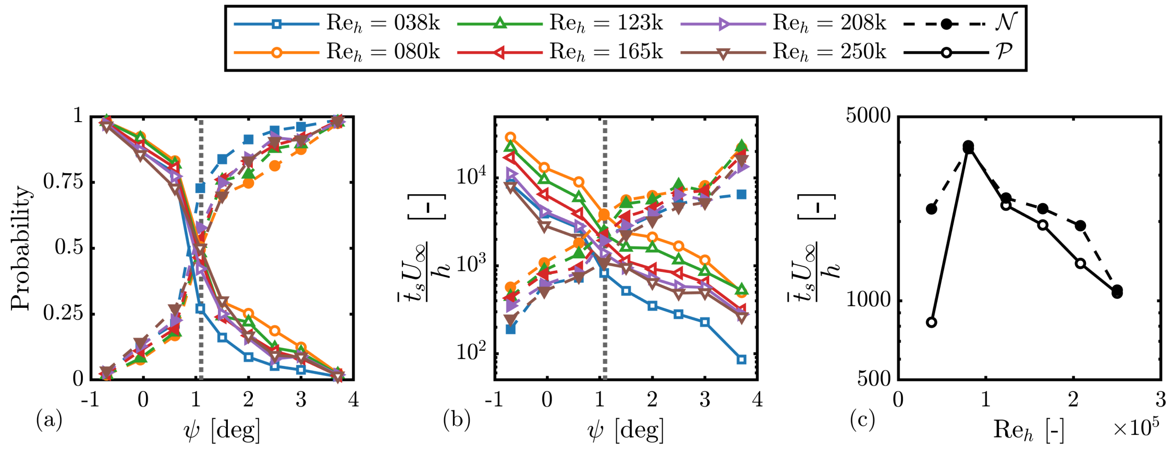

Figure 3. (a) probability of the flow being in either bi-stable state versus yaw angle, ψ. (b) the average residence time for each bi-stable state with change in ψ. (c) The average residence times at the $\psi = 1.1^\circ$ (data points at vertical dashed line in (a) and (b)) versus change in Re$_h$.

in the $\mathcal{P}$ state and on the $-z$ side of the hill for the $\mathcal{N}$ state. The identified switches can be used to determine the residence times, t_s, which is the time the flow remains in one state before switching to the other. The residence times are then grouped based on the state of the flow.

The bi-stability was tracked over a sweep of yaw angles to identify the range of ψ where the bi-stability was present. Each yaw angle tested was set with an accuracy of $\pm 0.1^\circ$. The average residence time, $\bar{t}_s$ scaled by U_∞ and h, and the probability of the flow being in either state over a range of ψ is presented in Figure 3. The bi-stability was found to be present over a 4.5° range, which is much larger than the 1° range seen with the Ahmed body (Volpe *et al.*, 2015; Haffner *et al.*, 2020). Smooth changes in curvature with the BeVERLI Hill provide a gradual transition in flow regime compared to the sharp trailing edges of the Ahmed body. At the extremes of this range, the flow is near being "locked-in" to one of the bi-stable states. The "locking-in" can be seen in the high probability and maximum $\bar{t}_s U_\infty / h$ for one state while other state is near zero probability with a minimum in $\bar{t}_s U_\infty / h$. Over the sweep in yaw-angle, $\bar{t} U_\infty / h$ changes exponentially up to two orders of magnitude. The sensitivity of the bi-stability to boundary conditions is demonstrated through the near even split between states occurring at $\psi \approx 1.1^\circ$, as opposed the nominally symmetric orientation 0°.

There is a non-monotonic trend between $\bar{t}_s U_\infty / h$ with respect to Re$_h$ for all ψ. An example of this trend is shown in Figure 3c for the measurements collected at $\psi = 1.1^\circ$. Starting at the lowest Reynolds number of 38,000, $\bar{t}_s U_\infty / h$ increases with Reynolds number up to a maximum at Re$_h = 80,000$. After this point, the trend decreases monotonically at an exponential rate with further increases in Reynolds number for the range tested. This differs from the trend reported previously by MacGregor & Lavoie (2024), where the peak in $\bar{t}_s U_\infty / h$ occurred at Re$_h = 123,000$ for the same set of Reynolds numbers. In these previous experiments, measurements were collected in conjunction with PIV and were of short duration (approximately two minutes) with several samples used to build the overall datasets of t_s. This approach captured short duration residence times only, which skewed $\bar{t}_s$ lower. As a result, the peak in $\bar{t}_s$ was detected at a higher Re$_h$. The present results rectify this by sampling continuously for $\mathcal{O}(10^5)$ times the convective time scale where a minimum of 175 successive bi-stable switch events are captured. It is hypothesized that the drop in $\bar{t}_s U_\infty / h$ at Re$_h = 38,000$ is due to a small change in flow regime, primarily that the flow separation occurs slightly more upstream compared to the other Reynolds numbers. The link between this earlier flow separation and its interaction with the bi-stability requires further investigations.

Bi-stability as a Stationary Markov Chain

Grandemange *et al.* (2013*a*) and Volpe *et al.* (2015) demonstrated that the bi-stability on the Ahmed body is a random process that behaves as a stationary Markov chain. They were able to prove this by showing that the following three conditions were satisfied:

1. the process must have a discrete number of states;
2. the distribution of residence times for each state must follow from an exponential distribution;
3. the memoryless condition must be satisfied, which requires the future state to depend solely on the current state.

These conditions were satisfied using datasets where the bi-stability was near evenly split between the two states. Thus, for a similar comparison with the Ahmed body, the datasets collected at $\psi = 1.1^\circ$, where the BeVERLI Hill bi-stability was near evenly distributed, are used.

The first condition listed is clearly satisfied for the BeVELRI hill since there are two distinct bi-stable states. The second condition can be verified by demonstrating for each state that the set of residence times can be generated from an exponential distribution defined with a parameter of $1/\bar{t}_s$. An equivalent approach is to compare the empirical distribution function (EDF) of t_s for each state against its corresponding cumulative distribution function (CDF) defined by $1/\bar{t}_s$. The quality of this match can be evaluated quantitatively using the Kolmogorov–Smirnov (KS) test as used by Volpe *et al.* (2015). This test calculates a parameter using the maximum difference between the EDF and CDF, and compares it to a tabulated threshold value for a given confidence level. For this analysis, a significance level of 0.05 is used. This test was passed for Re$_h$ less than or equal to 165,000 for both the $\mathcal{P}$ and $\mathcal{N}$ states. At higher Reynolds numbers (208,000 and 250,000), the threshold value was exceeded for the $\mathcal{P}$ state only. Closer examination of these cases found that the source of deviation was a localized mismatch from the CDF rather than a major departure from following the exponential distribution shape.

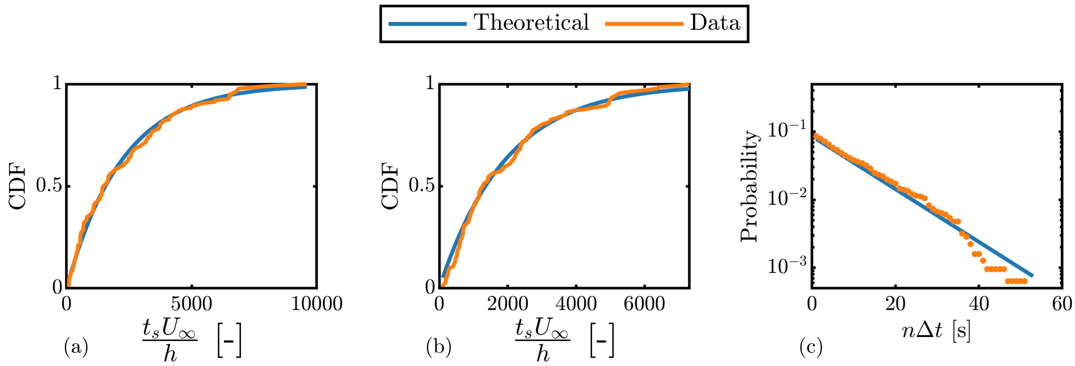

Figure 4. Stationary Markov chain test for $\text{Re}_h = 165,000$ at $\psi = 1.1°$. (a) and (b) show for $\mathcal{N}$ and $\mathcal{P}$, respectively, the empirical distribution function of residence times for each bi-stable state compared against their corresponding theoretical cumulative distribution function that is based on the rate parameter of $1/\bar{t}_s$. (c) compares the measured probability distribution against the theoretical probability expression of Equation 2.

Thus, the second condition of the stationary Markov chain analysis can be taken to be satisfied. The EDF and CDF comparison for $\text{Re}_h = 165,000$ is presented in Figure 4a and 4b.

To verify the third condition, several probabilistic quantities need to be calculated. A probability will be denoted as Pr with the vertical bar denoting conditional probability. The state of the flow after i fixed increments, Δt, is denoted as $\mathcal{S}_i$, where $i = 0$ is the current time. For this analysis Δt is set at 1 s. The first probabilities that need to be determined are $\text{Pr}(\mathcal{S}_0 = \mathcal{P})$, $\text{Pr}(\mathcal{S}_0 = \mathcal{N})$, $\text{Pr}(\mathcal{S}_1 = \mathcal{N}|\mathcal{S}_0 = \mathcal{P})$, and $\text{Pr}(\mathcal{S}_1 = \mathcal{P}|\mathcal{S}_0 = \mathcal{N})$. All of these probabilities can be determined by tracing through the bi-stability parameter signal at a rate of $1/\Delta t$ taking the current point in the signal as $i = 0$. Grandemange *et al.* (2013*a*) showed that these probabilities can then be used in

$$\begin{aligned} \text{Pr}_s = \text{Pr}(\mathcal{S}_1 = \mathcal{P}|\mathcal{S}_0 = \mathcal{N}) \cdot \text{Pr}(\mathcal{S}_0 = \mathcal{N}) \\ + \text{Pr}(\mathcal{S}_1 = \mathcal{N}|\mathcal{S}_0 = \mathcal{P}) \cdot \text{Pr}(\mathcal{S}_0 = \mathcal{P}) \end{aligned} \quad (1)$$

to determine the probability of the flow switching states after Δt. Then, with Pr_s known, the probability of the flow changing states after n increments of Δt can be determined using

$$\text{Pr}(\mathcal{S}_{n+1} \neq \mathcal{S}_i \; \forall \; i \in \{0,...,n\}) = \text{Pr}_s \cdot (1 - \text{Pr}_s)^n. \quad (2)$$

Figure 4c shows the comparison of this theoretical probability against the experimentally measured counterpart. The experimental results can be determined using the same approach to determine the base probability quantities. There is currently no quantitative measure to evaluate the match between these trends, so a qualitative visual check is made instead. There is strong agreement between the two trends indicating that this condition is also met. Fewer samples are available at larger $n\Delta t$ resulting in the observed deviation of the measurements from the experimental trend. Hence, with the three conditions met, the bi-stability seen on BeVERLI Hill is indeed a random process that behaves as a stationary Markov chain.

Breathing of the Recirculation Region

The breathing of the recirculation region was first noticed in the second POD mode from the unsteady surface-pressure measurements. Snapshots of the flow field along the centerline of the leeward face of the hill were spatially filtered using a 40% energy POD reconstruction method. A sample snapshot of the POD filtered field is shown in Figure 5a with the $0.5U_\infty$ line within the separated shear layer indicated by the white dashed line. The wall-normal position of this velocity line at each streamwise position with velocity vector information was tracked across all snapshots. A PDF of the wall-normal position of this line was generated for each streamwise position. For visualization purposes, Figure 5b shows these 1D distributions normalized by their maximum value (note that the PDFs no longer integrate to an area of 1). Under this approach, the average position of the $0.5U_\infty$ line is indicated where the distribution is equal to one with the range of wall-normal positions at each streamwise position.

In Figure 5a, a circle and cross are used to indicated the position of a pressure port at $(x/h, y/h, z/h) = (0.68, 0.95, 0)$ that is connected to an Endevco transducer and a hot-wire at $(1.75, 0.8, 0)$ within the separated shear layer. The premultiplied spectra from the hot-wire is shown in Figure 5c with peaks at $\text{St}_h = 0.065$ and $\text{St}_h = 0.65$. The first peaks aligns with the recirculation region breathing highlighted in the POD measurements. The other peak centred at $\text{St}_h = 0.65$ aligns with the development of a shear layer instability. The magnitude-squared-coherence (MSC) between the hot-wire and unsteady surface-pressure signal is shown in Figure 5d, where a strong match is seen at $\text{St}_h = 0.065$ indicating that the movement of the shear layer is tied to the fluctuations seen in the surface-pressure. No coherence is seen for the higher frequency peak indicating that it only develops once the shear layer has separated from the hill.

CONCLUSIONS

The low-frequency dynamics of the BeVERLI Hill wake were explored through a combination of unsteady surface-pressure, HWA and PIV measurements. A large scale, bi-stable mode alternates randomly between two mirror-symmetric states at large time scales. This random switching was found to behave as a stationary Markov chain when the flow is near evenly split between the two states. The average time scale of bi-stability ranged between $\mathcal{O}(10^2 - 10^4)$ times the convective time scale of the flow depending on the yaw angle orientation of the hill. Variation in this time scale with Re_h was found to be non-monotonic for the range of Reynolds numbers tested with a peak value observed at $\text{Re}_h = 80,000$. The bi-stability was found to be present over an approximately 4.5° range with an even split between states occurring at ap-

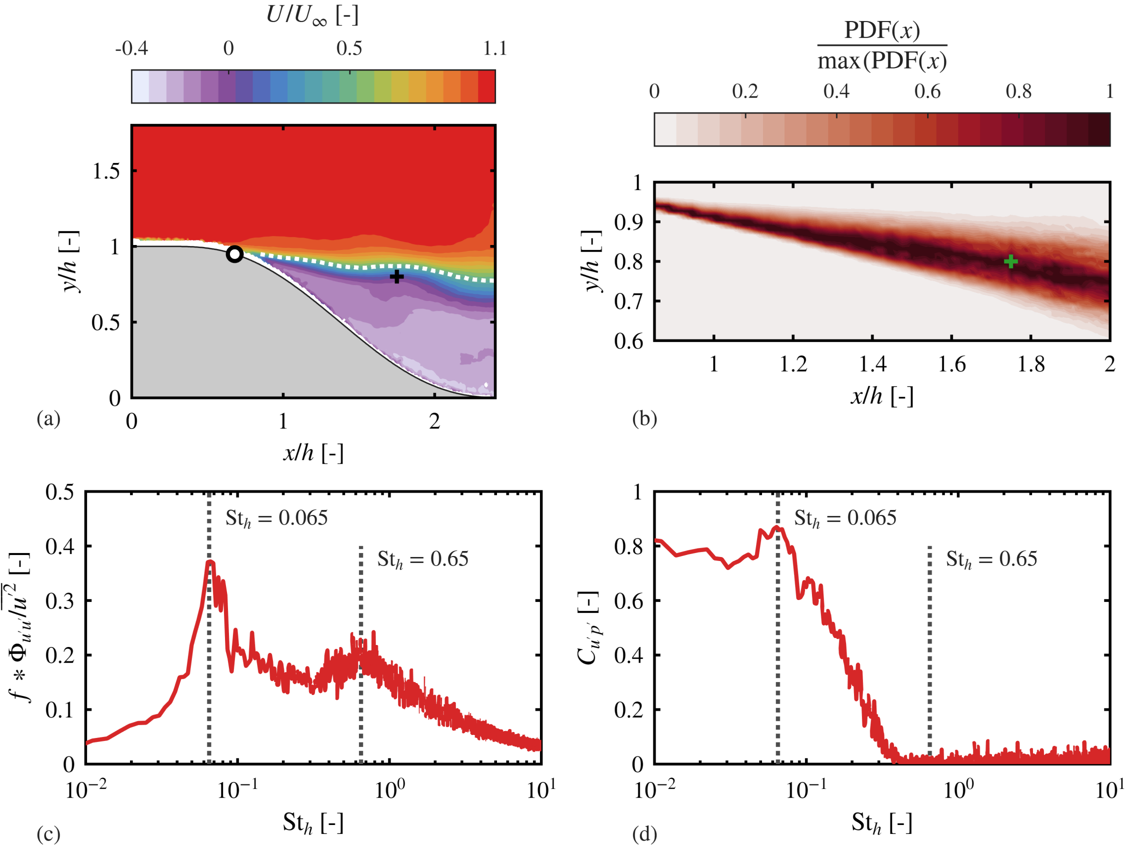

Figure 5. Results for $\mathrm{Re}_h = 165{,}000$ at $\psi = 0°$. (a) Sample snapshot of 40% energy reconstructed streamwise velocity along the model centerline with the $0.5U_\infty$ line indicated by the dashed white line. The position of the pressure port and hot-wire used to produce (c) and (d) are indicated with a circle and cross, respectively. (b) Contour mapping to visualize the range of shear layer positions via the PDFs of y/h position of the $0.5U_\infty$ for each streamwise position normalized by its max(PDF). (c) Pre-multiplied spectra of the velocity measured by the hot-wire. (d) Magnitude-square-coherence of fluctuating pressure and velocity measured by the hot-wire.

proximately 1.1° instead of 0°. This offset in yaw angle is attributed to the sensitivity of the bi-stability to installation effects and boundary conditions. A breathing of the recircualtion region was observed at $\mathrm{St}_h = 0.065$ through unsteady surface-pressure measurements. The movement of the shear layer along the centreline of the hill due to this mode was determined through HWA. Additionally, HWA identified the development of a shear layer instability at $\mathrm{St}_h = 0.65$.

REFERENCES

Berger, E., Scholz, D. & Schumm, M. 1990 Coherent vortex structures in the wake of a sphere and a circular disk at rest and under forced vibrations. *Journal of Fluids and Structures* **4** (3), 231–257.

Duetsch-Patel, J. E., MacGregor, D., Jenssen, Y. L., Henry, P.-Y., Muthanna, C., Savio, L., Lavoie, P., Gargiulo, A., Sundarraj, V., Ozoroski, T. A., Roy, C. J., Devenport, W. J., Borgoltz, A. & Lowe, T. 2022 The BeVERLI Hill three-dimensional separating flow case: Cross-facility comparisons of validation experiment results. In *AIAA SciTech 2022 Forum*, pp. AIAA–2022–0698. San Diego, CA & Virtual: American Institute of Aeronautics and Astronautics.

Gargiulo, A., Beardsley, C., Vishwanathan, V., Fritsch, D. J., Duetsch-Patel, J. E., Szoke, M., Borgoltz, A., Devenport, W. J., Roy, C. J. & Lowe, K. T. 2020 Examination of flow sensitivities in turbulence model validation experiments. In *AIAA Scitech 2020 Forum*, pp. AIAA–2020–1583. Orlando, FL: American Institute of Aeronautics and Astronautics.

Grandemange, M., Gohlke, M. & Cadot, O. 2013*a* Bi-stability in the turbulent wake past parallelepiped bodies with various aspect ratios and wall effects. *Physics of Fluids* **25** (9), 095103.

Grandemange, M., Gohlke, M. & Cadot, O. 2013*b* Turbulent wake past a three-dimensional blunt body. Part 1. Global modes and bi-stability. *J. Fluid Mech.* **722**, 51–84.

Haffner, Y., Borée, J., Spohn, A. & Castelain, T. 2020 Mechanics of bluff body drag reduction during transient near-wake reversals. *J. Fluid Mech.* **894**, A14.

Hearst, R. J. 2015 Fractal, classical, and active grid turbulence: From production to decay. PhD thesis, University of Toronto.

MacGregor, D. & Lavoie, P. 2024 On the structure and behaviour of the wake behind a three-dimensional hill. In *13th International Symposium on Turbulence and Shear Flow Phenomena (TSFP13)*. Montreal, Canada.

MacGregor, D. A., Gargiulo, A., Duetsch-Patel, J. E., Lavoie, P. & Lowe, T. 2023 Mean and unsteady surface-pressure measurements on the BeVERLI Hill. In *AIAA SciTech 2023 Forum*, pp. AIAA–2023–0468. National Harbor, MD & Online: American Institute of Aeronautics and Astronautics.

Volpe, R., Devinant, P. & Kourta, A. 2015 Experimental characterization of the unsteady natural wake of the full-scale square back Ahmed body: Flow bi-stability and spectral analysis. *Exp Fluids* **56** (5), 99.

Williams, O. J. & Smits, A. J. 2024 Asymmetries in nominally symmetric flows. *Annual Review of Fluid Mechanics* **57**, 35–60.